Acta Scientiarum

http://periodicos.uem.br/ojs/acta
ISSN on-line: 1807-8664
Doi: 10.4025/actascitechnol.v42i1.41102

In vitro and *in vivo* response of composites based on chitosan, hydroxyapatite and collagen

Maurício Bordini do Amaral[1], Rommel Bezerra Viana[2*], Katúcia Bezerra Viana[3], Cristina Aparecida Diagone[4], Aline Bassi Denis[4] and Ana Maria de Guzzi Plepis[4]

[1]Departamento de Bioengenharia, Universidade de São Paulo, São Carlos, São Paulo, Brazil. [2]Instituto de Química, Universidade Federal de Alfenas, Avenida Jovino Fernandes Salles, 2600, 37133-840, Alfenas, Minas Gerais, Brazil. [3]Centro de Ciências Biológicas e da Saúde, Universidade Federal do Estado do Rio de Janeiro, Rio de Janeiro, Rio de Janeiro, Brazil. [4]Instituto de Química de São Carlos, Universidade de São Paulo, São Carlos, São Paulo, Brazil. *Author for correspondence. E-mail: rommelbv@yahoo.com.br

ABSTRACT. The goal of this study was to evaluate the in vitro cellular toxicity and biological behavior of new bone graft composites after subcutaneous implantation during remodeling and wound-healing processes. We developed composites based on hydroxyapatite (obtained by deproteinizing bovine bone), collagen (obtained from bovine tendon) and chitosan (obtained from gladii of the squid species Loligo), that were characterized by different techniques (X-ray, FT-IR, Thermogravimetry, DSC and SEM). Three biomaterials were evaluated here: B1 (collagen/chitosan/hydroxyapatite), B2 (collagen/hydroxyapatite) B3 (collagen/hydroxyapatite). For *in vitro* cytotoxicity tests, two cell lines were used: HEp human larynx tumor cells (ATCC-CCL-23) and VERO cells from African green monkey (*Cercopithecus aethiops*). These toxicity tests demonstrated that the evaluated composites are not toxic. In biocompatibility tests, the results of a histological analysis showed that all three biomaterials present a low inflammatory tissue reaction. The tissue response was most favorable for sample B3, followed by B2 and B1, in that order. Based on these results, we conclude that all three biomaterials show good biocompatibility and no evidence of cytotoxicity; thus, these materials represent good candidates for tissue and graft engineering for use in bone regeneration.

Keywords: scaffolds; tissue regeneration; immunohistochemistry; chitosan; hydroxyapatite; collagen.

Received on December 27, 2017.
Accepted on October 18, 2018

Introduction

There are many clinical reasons to develop biomaterials, especially for use in bone tissue. Biomaterials for bone tissue are used, for example, in the filling of extensive bone defects (Bongio, van den Beucken, Leeuwenburgh, & Jansen, 2015) and in the development of implants that will be subjected to mechanical forces with applications in orthopedics (Ong, Yun, & White, 2015), odontology (Li, Chow, & Matinlinna, 2014), and oral and maxillofacial surgery (Keranen et al., 2011). In this context, it is important to emphasize that the advancement of the dentistry science was accompanied by the development of biomaterials, from their manufacturing to understanding the obtained cellular responses (Shin, 2007).

Collagen and hydroxyapatite are well known compounds applied in tissue engineering research. Few studies (Zhou & Lee, 2011; Sadat-Shojai, Khorasani, Dinpanah-Khoshdargi, & Jamshidi, 2013) have reported the preparation of hydroxyapatite/Collagen microspheres as a potential material for filling bone and periodontal cavities. Sato, Kikuchi, and Aizawa (2017) developed a hydroxyapatite/collagen injectable bone paste with an anti-washout property, and Choi, Kim, Jo, Koh, and Kim (2017) reported a self-assembly-induced gelation approach for hydroxyapatite/collagen composite microspheres with a nanofibrous structure to be used as bone scaffolds. Recently, Calabrese et al. (2017) evaluated a hydroxyapatite/collagen scaffold inducing bone formation after subcutaneous implantation in mice and the influence of human mesenchymal stem cells in the ectopic bone formation, while Begam, Nandi, Chanda, and Kundu (2017) assessed the effect using bone morphogenetic protein-2. Moreover, the stabilizing effect in hydroxyapatite/collagen scaffolds by incorporating carbodiimide (Kozlowska, Sionkowska, Osyczka, & Dubiel, 2017), graphene oxide (Wang et al., 2017), carbon nanotube (Jing et al., 2017), calcium phosphate (Zhao et al., 2017), PLGA and alginate microparticles (Quinlan et al., 2015) were also performed to improve the mechanical and biological properties.

Another important issue is the triple composites based on a hydroxyapatite/collagen/chitosan formulation. Huang (Huang et al., 2011a; Huang, Feng, Yu, & Li, 2011b; Huang et al., 2011c) developed a nano-sized hydroxyapatite minerals and type I collagen matrix loaded chitosan injectable scaffold with or without mesenchymal stem cells into bone defects showing that this can be a potential approach for reconstruction of irregular bone defects. On the other hand, the evaluation a hydroxyapatite/collagen/chitosan composite as a potential maxillofacial reconstruction material after simulated body fluid immersion were performed by Verisqa, Triaminingsih, and Corputty (2017) and Sari, Indrani, Johan, and Corputty (2017), while the injectability, thermo-irreversible properties of hydroxyapatite/collagen/chitosan loaded with glycerophosphate was reported by Huang, Tian, Yu, Xu, and Feng (2009). In addition, Chen et al. (2012) studied the injection process of a hydroxyapatite/ collagen/chitosan hydrogel directly and noninvasively applying a ultrasound methodology to elucidate the quantitative *in vivo* reactions in the tissue development. Teng, Liang, Wang, and Luo (2016) developed hydroxyapatite/collagen/chitosan composite microspheres with narrow particle distribution, while some studies have studied the addition of nano-sized hydroxyapatite into blends based on collagen/chitosan/(hyaluronic acid) in order to understand their mechanical parameters and thermal stability (Sionkowsk & Kaczmarek, 2017), as well as a support in tissue engineering and regenerative medicine (Kaczmarek, Sionkowsk, & Osyczka, 2017)

The purpose of this study was to characterize and study the biological behavior of composites based on polyionic collagen, natural hydroxyapatite and chitosan that are intended for use in bone tissue reconstruction. Then, hydroxyapatite/collagen/chitosan (B1) and hydroxyapatite/collagen composites (B2, B3) were developed to further biological tests. Hydroxyapatite was obtained here by deproteinizing bovine bone with particle sizes ranging from lower than 0.20 to 1.18 mm, contrary to previous works that applied nano-sized hydroxyapatite minerals (Huang et al., 2011a; 2011b; 2011c; Chen et al., 2012). In the case of chitosan, the samples here were extracted from gladii of the squid species *Loligo vulgaris*, instead of incorporating chitosan gel from crab shell or obtained by commercial chitosan powder samples. These materials and biomaterials were subjected to characterization using X-ray, FT-IR, Thermogravimetry, Differential Scanning Calorimetry (DSC), and Scanning Electron Microscopy (SEM). Furthermore, HEp human larynx tumor cells (ATCC-CCL-23) and normal kidney cells (VERO) from African green monkey (*Cercopithecus aethiops*) were used for *in vitro* cytotoxicity tests. In the *in vivo* biocompatibility tests, the samples were implanted subcutaneously in the dorsal region of 51 Wistar rats and the tissue effects were evaluated by histological analyses.

Material and methods

Hydroxyapatite was obtained by deproteinizing bovine bone. After removing tissues and residues, the bone was cut into 1-cm^3 cubes (of the portion corresponding to trabecular bone), washed with H_2O_2 to remove free albumin, and then washed with ethanol. Subsequently, the bone was left in contact with H_2O_2 at room temperature, after which it was autoclaved. The process was repeated until the amount of residual organic mass reached 12%. The bone was then washed with water, dried at 100 and calcined at 800°C. The cubes were then pulverized, with particle sizes ranging from 0.20 to 1.18 mm.

Bovine tendon was the source of collagen gel. After washing tendon with saline solution (0.9%) to remove blood, the tendon was shredded and treated with an alkaline solution containing DMSO/H_2O and Na^+, K^+, and Ca^{++} salts (chlorides and sulfates) [Goissis, Piccirilli, Plepis, & Das-Gupta, 1999]. After 24 hrs, the alkaline solution had stabilized, and residual salts were removed by successive washings with H_3BO_3 (3%) and EDTA (3%); the solution was finally extracted with an acetic acid solution (pH 3.5). This final solution was deaerated and stored at 4°C.

Chitosan was obtained from gladii of the squid species *Loligo vulgares*. The preparation of chitosan from β-chitin was based on the Kurita process (Goissis et al., 1999), which consists of demineralization in acid medium (HCl 0.55 mol L^{-1}), deproteinization in alkaline medium (NaOH 0.30 mol L^{-1}), and deacetylation in NaOH 40% (w w^{-1}). A 0.5% chitosan solution was prepared by dissolving chitosan in a solution of acetic acid (1%) in deionized water. The obtained chitosan had an acetylation degree of 16.3%, similar to results obtained in other studies (Horn, Martins, & Plepis, 2009; Horn, Martins, & Plepis, 2010). All biomaterials used in this study were sterilized using ethylene oxide.

Three matrices were prepared; throughout this manuscript, these matrices will be referred to as mats B1, B2, and B3. Biomaterial B1 was formed by a mixture of powdered hydroxyapatite and a collagen:chitosan blend at a ratio of 2:1 (w w^{-1}) (Attaf, 2011). This blend was obtained by mixing collagen gel (1%) and chitosan solution (0.5%) at a ratio of 1:1 (w w^{-1}). The hydroxyapatite used was a mixture of particles with sizes between 0.25 and 1.18 mm (1:1). B2 was composed of powdered hydroxyapatite and collagen gel (1%) at a ratio of 1:5 (w w^{-1}) (Attaf, 2011); the same mixture of hydroxyapatite particles used in B1 was also used for B2. In the case of B3, this biomaterial was composed of powdered hydroxyapatite and collagen gel (1%) at a ratio of 1:5 (w w^{-1}); however, the hydroxyapatite used was a mixture of particles of sizes smaller than 0.2 mm.

In order to obtain scanning electron microscopy (SEM) photomicrographs, the biomaterials were frozen and freeze–dried. Subsequently, the biomaterials were placed on appropriate supports and covered with a thin layer of gold/palladium (thickness, 20 nm). The materials were sputter-coated using a Balsers sputter coater (model SDC 050), and photomicrographs were recorded using a ZEISS microscope (model LEO-440). Infrared analyses were carried out using a Fourier–Transform InfraRed (FT-IR) spectrophotometer (NEXUS 670 FT-IR/Nicolet – ns - AEQ0000517). TG-DTA experiments were performed in a SDT-Q600 Simultaneous Thermogravimetric Analyzer (TA Instruments), using an alumina sample holder under air atmosphere at a flow rate of 100 mL $min.^{-1}$. The temperature ranged from 25 to 800°C at a 10°C $min.^{-1}$ heating rate. In addition, a DSC-Q10 modulus (TA Instruments) was used to differential scanning calorimetric measurements. The DSC curves were obtained under a dynamic nitrogen atmosphere (50 mL $min.^{-1}$) in the temperature range of -80 to 250ºC at a 10ºC $min.^{-1}$ heating rate.

The *in vitro* cytotoxicity test was carried out using the agar diffusion method, following Rogero (Rogero, Higa, Saiki, Correa, & Costa, 2000; Rogero, Lugao, Ikeda, & Cruz, 2003) methodology. Two cell lines were used: HEp human larynx tumor cells (ATCC-CCL-23) and normal kidney cells (VERO) from African green monkey (*Cercopithecus aethiops*). The biomaterials were evaluated together with the positive control (latex), and both of these were extracted according to the ISO10993-5 standard. The cells were seeded at a concentration of 3 x 10^5 per mL^{-1} in a Petri dish (15 x 60 mm) in a volume of 5 mL and incubated for 48 hours at 37°C in a humid atmosphere containing 5% CO_2. When a monolayer of cells had formed, the culture medium was discarded, and 5 mL of the overlay medium was added to each Petri dish (this procedure was conducted in a laminar flow chamber. The medium comprised equal parts Eagle minimum essential medium (MEM) and 1.8% agar containing 0.01% of neutral red. The agar was melted and mixed in equal proportions with MEM at 44°C. Fragments of the three materials were placed on top of the agar before full solidification, and each had a surface area of 0.25 cm^2. The Petri dishes were incubated once again in an incubator under 5% CO_2 at 37°C for 24 hours. In addition, two controls were used for the agarose-based experiment, a positive and a negative one. Latex fragments were used as a positive control, while the negative control was non–toxic filter paper disks with a surface area of 0.25 cm^2. Each material was duly selected in 3 mm x 4 mm x 6 mm pieces and submerged in 2 mL of MEM for 24 hours under static conditions at 37°C. Using DMEM for the VERO cells (1x10^5 cells per mL^{-1}) and Eagle medium for the HEp-2 cells (containing 10% SFB), the cells were placed into a 96–well microtiter plate, which was then incubated at 37°C under 5% CO_2. After 24 hours, the medium was removed by aspiration, and the cell monolayer was washed using PBS. The extract solutions were prepared in a medium containing 3% SFB in the absence of phenol red at concentrations of 100, 90, 75, 60, 50, 25, and 10%. These solutions were prepared using the biomaterial extracts. The cells were incubated for 24 hours with the extracts in a 96–well plate at 37º C under 5% CO_2 (in triplicate). This cell counting method is based on the reduction of 3-(4,5-dimethylthiazol-2-yl)-2,5-diphenyltetrazolium bromide (MTT) (yellow) to formazan (purple), which absorbs light at 570 nm. MTT is reduced by mitochondrial dehydrogenases, which are found only in live cells (Taylor, Papp, & Pollard, 1994; Taylor, Cuff, Leger, Morra, & Anderson, 2002). After 3 hours of incubation, the MTT medium was removed, and 50 µL of pure ethanol was added. After complete dilution, 150 µL of PBS was

added with isopropanol at a ratio of 1:1. The plates were measured using an ELISA BIO-RAD reader at 550 nm. The results are presented in the form of absorbance plots and are presented as a function of the concentration of the biomaterial extract.

For the in vivo biocompatibility tests, a total of 51 adult (approximately 70 days old/approximate weight of 250 g) male albino Wistar rats (*Rattus norvegicus*) were randomly divided into three groups of 17, with each group corresponding to each one of the three tested biomaterials. These groups were further divided according to the postsurgical period: 3, 7 and 28 days (n = 5 rats). Two control animals were used for each group: the first animal did not undergo the surgical procedure, and the second animal underwent the surgical procedure, but the biomaterial was not implanted. The same surgical sequence was followed for all animals (see Figure 1). All animals were anesthetized using a 1:1 mixture of ketamine hydrochloride (injectable *Ketalar–Achë Laboratórios Farmacêuticos S.A.*), at a dose of 75 mg kg^{-1} of body mass, and the muscle relaxant and animal sedative Ropun (Bayer S.A.) was applied intramuscularly at a dose of 1.5 mL kg^{-1}. The animals were then placed on a sterile surface for the surgical procedure. The dorsal areas of the animals were shaved (following the sagittal line) to expose the skin and then disinfected with gauze soaked with povidone–iodine (PvPi). Using a surgical scalpel blade No.15, a straight, 1.5-cm incision was performed on the right side, parallel to the mid–sagittal line (exposing the subcutaneous tissue). Next, the subcutaneous space was divulsed to produce a pouch; the incision edges were then separated, and the biomaterial was introduced in the subcutaneous space, approximately 1 cm from the incision. The biomaterials had a size of 1x10x10 mm. The incision edges were reapproximated and sutured using 4.0 Ethicon silk thread (Johnson & Johnson). After the suture was complete, post–operation disinfection was carried out using PvPi. One biomaterial was placed per animal, following the previously described group distribution. The animals remained in the animal house, where they received feed and water *ad libitum* throughout the experiment. Once the predefined experimental periods for each group were complete, the animals were once again anesthetized and then killed using an intramuscular infiltration of potassium chloride, followed by disinfection with PvPi. After locating the biomaterials, incisions were performed using the appropriate safety margin, and the material and the adjacent tissue were carefully removed. Immediately after removal, the material was pinned onto a polystyrene board (to avoid morphological alterations in the tissue) and immersed in a 10% formaldehyde phosphate-buffered solution (pH 7) for 72 hours for tissue fixation. The histological sections were then subjected to HE (hematoxylin/eosin) staining. Immunohistochemistry was performed to evaluate the presence of macrophages.

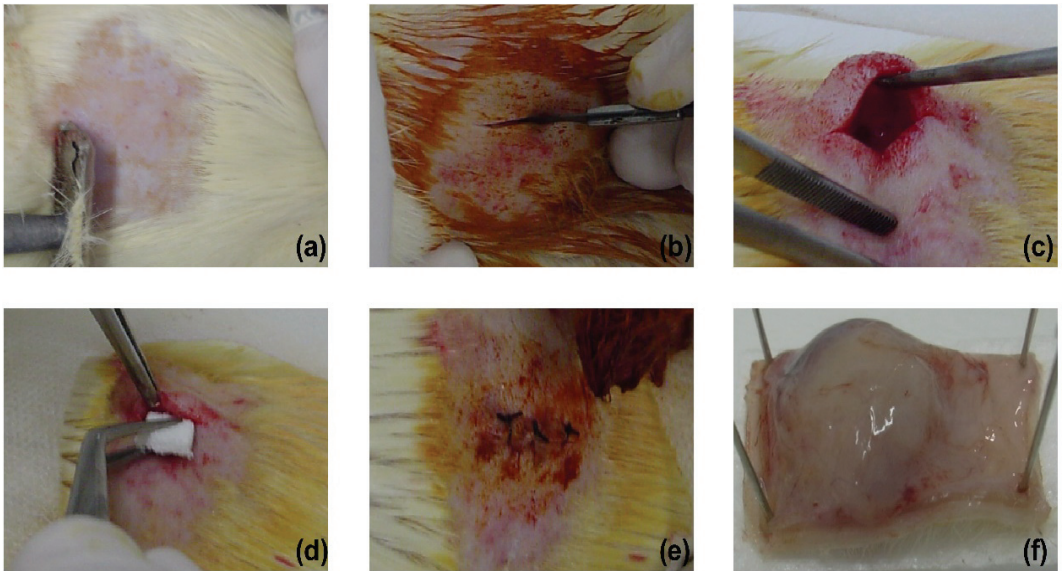

Figure 1. (a)-(c): after shaving and disinfection, incisions and subcutaneous pockets were made on the left back. (d)-(e): suture was made after biomaterials injection on pockets. (f): at various time points the rats were sacrificed and the implants and surrounding tissue were dissected and fixed with 10% formalin.

The sections were evaluated using a Leica Leitz DM RX microscope and the attached image analysis system. For histological analysis, the tissue reaction to the implants was graded according to the following semi–quantitative system: (-) no reaction, (+) minimal reaction, (++) moderate reaction, (+++) well–established reaction, and (++++) intense reaction. The tissue reaction results are described in Table 1. The following parameters were considered for this grading system: (a) the presence of an inflammatory infiltrate, which refers inflammatory cells such as lymphocytes, plasmocytes and polymorphonuclear leukocytes (PMN); (b) the presence of a fibrin network around the implant; (c) neovascularization, which refers to the presence of blood vessels around the implants; (d) the thickness and quality of the fibrous capsule; (e) internal cell growth; and (f) the evaluation of the macrophages.

Table 1. Semi–quantitative grading system for the evaluation of the tissue reaction to the implants during the histological analyses.

Response	Tissue reaction to the implants during the histological analyses
	Inflammatory infiltrate
(-)	Absence of inflammatory cells
(+)	minimal inflammatory response, with the presence of one or a few cells
(++)	moderate inflammatory response, with few cell groups present
(+++)	marked inflammatory response, with the presence of several agglomerates of inflammatory cells
(++++)	intense inflammatory response, with a strong presence of inflammatory cells throughout the tissue
	Fibrin network around the implant
(-)	absence of fibrin
(+)	very thin fibrin network
(++)	small fibrin network
(+++)	average fibrin network
(++++)	intense thick fibrin network
	Neovascularization
(-)	Absence of blood vessels
(+)	presence of a few blood vessels
(++)	moderate presence of blood vessels
(+++)	presence of several blood vessels
(++++)	presence of many blood vessels around the implant
	Quality of the fibrous capsule
(-)	absence of fibrous capsule
(+)	presence of a few inflammatory cells, with little or no organized conjunctive tissue
(++)	capsule tissue is granulomatous and dense, containing fibroblasts and some inflammatory cells
(+++)	capsule tissue is fibrous, although immature, presenting fibroblasts and little collagen
(++++)	mature, dense and well-established fibrous capsule
	Internal cell growth
(-)	absence of cells inside the implant cracks
(+)	minimal presence of cells inside the implant cracks
(++)	moderate presence of cells in the implant cracks
(+++)	marked presence of cells in the implant cracks (fibrous tissue around the implant fragments)
(++++)	widespread degradation and almost complete fragmentation of the implant
	Macrophages
(-)	absence of macrophages
(+)	moderate presence of macrophages
(++)	presence of a macrophage layer
(+++)	presence of craters with macrophages in the biomaterials
(++++)	strong presence of macrophages in giant cells

Results and discussions

Characterization

The hydroxyapatite used in this study was initially compared with a standard hydroxyapatite sample, and both samples showed the same pattern. Thermogravimetric analysis of our hydroxyapatite samples showed a 0.51% loss of mass, which was related to the water present in the sample (see Figure 2); this loss was observed from 25 to 200°C. In the 200-400°C range, 0.48% of the organic matter remaining in the sample was degraded, and in the 400-700°C range, 0.45% of the material was carbonized, yielding a residue of 98.6%; these results indicate the purity of the hydroxyapatite samples used.

In the thermogravimetric analysis of the collagen sample, we observed a mass loss of 15.1%, which was related to the water present in the collagen (this loss was observed from 25 to 200°C). Approximately 42% of the collagen structure was degraded in the 200-400°C range. In the 400-700°C range, 41.8% of the material was carbonized, yielding a residue of 0.09%. We also performed a DSC analysis for collagen (see Figure 2f). The DSC results show the thermal transition of collagen at 41.6ºC, indicating that the collagen structure was not denatured during preparation (a thermal transition is not observed for denatured collagen). For the chitosan sample, a mass loss of 12.1% was observed in the 25-200°C range, which is related to the water present in the chitosan. In the range from 200 to 400°C, approximately 41.8% of the chitosan polymer chains were thermally degraded, and in the 400-700°C range, 46.1% of the material was carbonized (leaving no residue).

Examining the thermogravimetric analyses of the composites, a mass loss of 2.1% (which is related to the water present in biomaterial B1) was observed in the 25-200°C range; similarly, a mass loss of 1.5% was observed for biomaterial B2. In the 200-400°C range, approximately 3.5% of the organic matter was degraded in B1 and 4.2% was degraded in B2. In the 400-700°C range, 1.7 of B1 and 2% of B2 were carbonized, leaving residues of 92.2 and 92.5%, respectively. The losses observed at lower temperatures for B1 are due to the presence of chitosan in this biomaterial.

The infrared absorption spectra are shown in Figure 3. For the hydroxyapatite sample, absorption bands corresponding to the OH group can be observed at 3568 and 634 cm^{-1}, and the absorption of the PO_4^{3-} group can be detected at 1095, 1031, 961, 603, and 563 cm^{-1}. The infrared spectrum of the collagen sample shows bands at 1658 and 1550 cm^{-1}, corresponding the C=O axial deformation and the NH angular deformation of amides I and II, respectively. The absorption in the 600-800 cm^{-1} region for collagen is due to NH angular deformation. The integrity of the triple–helix structure of the collagen can be observed through the absorbance ratios measured at 1235 and 1450 cm^{-1}, which are related to the amide III band (C-N stretching and NH deformation) and to the CH bond of the pyrrolidine ring, respectively. The band at 3450 cm^{-1} is due to collagen OH stretching. Peaks at 1070 and 1030 cm^{-1} are observed in the chitosan infrared spectrum and are due to CO stretching. The band at 3450 cm^{-1} corresponds to OH stretching in the chitosan. The amide I and II bands of chitosan can be observed at 1650 and 1560 cm^{-1}, respectively. The intense band between 800 and 1200 cm^{-1} is due to the pyranoside rings [Horn et al., 2009, Huang et al., 2011b].

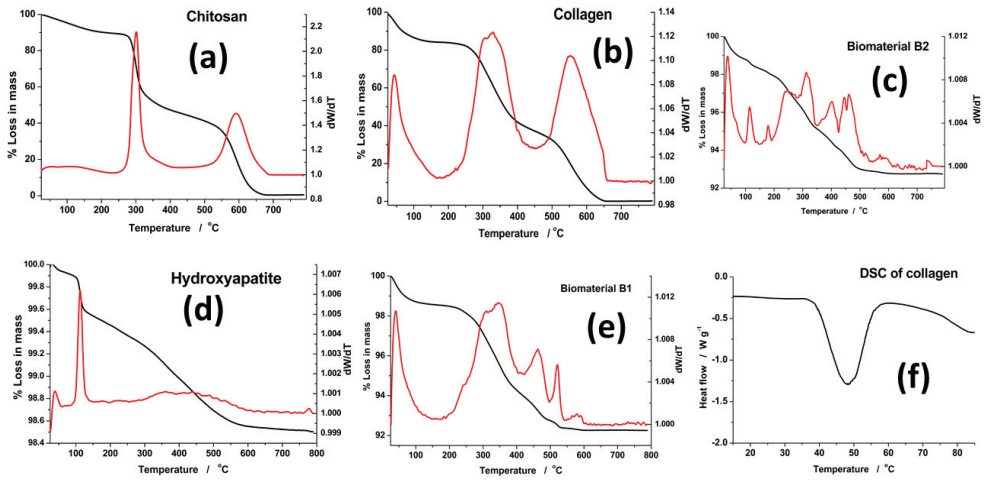

Figure 2. Thermogravimetric curves and their respective derivatives for (a) chitosan, (b) collagen (c) biomaterial B2, (d) hydroxyapatite and (e) biomaterial B1 samples. In (f) is shown the DSC spectrum of the collagen sample.

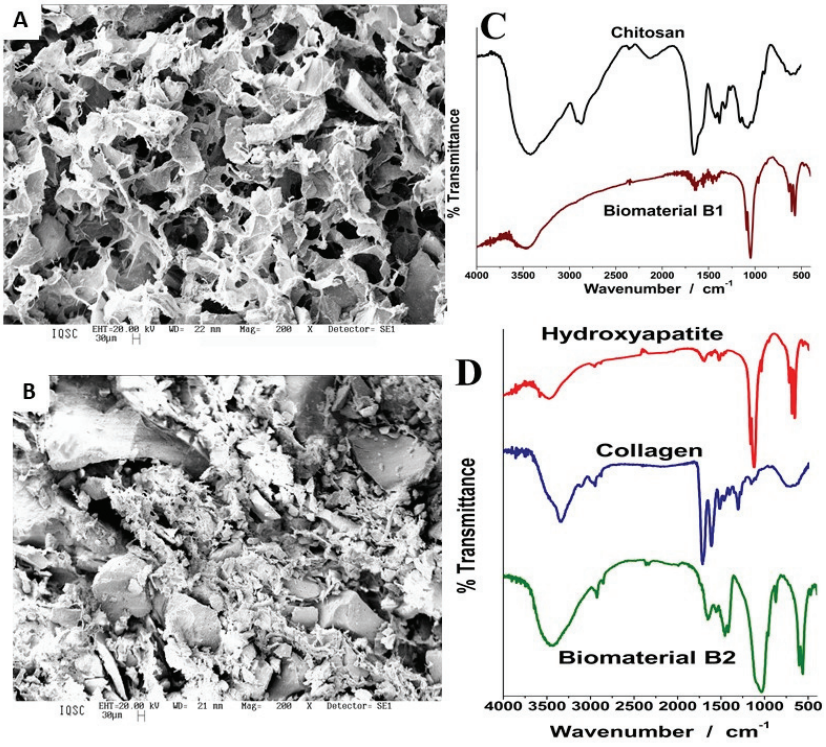

Figure 3. SEM micrographs of biomaterials B1 (A, at the top) and B2 (B, at the bottom) are shown in the left side. FT-IR spectra are shown in the right side. (C) Spectra of chitosan (in black, on the top) and biomaterial B1 (in purple, on the bottom). (D) Spectra of collagen (in blue, on the top), hydroxyapatite (in red, in the middle section) and biomaterial B2 (in green, on the bottom).

The infrared absorption spectrum of B2 (HA:Col) shows bands that are characteristic of hydroxyapatite and bands corresponding to the structure of collagen and that the change in the intensity of the bands in the B2 spectrum were very small when compared with the pure collagen spectrum. For B1 (HA:Col:CS), the same bands were observed, although a widening of the band in the 3000 cm^{-1} region was observed due to the presence of chitosan. Therefore, both spectra show bands that are characteristic of the materials used, indicating that no new material was obtained; only a mixture of the two original materials was detected. This is even more evident considering the preservation of the band intensities and the absence of new bands in the isolated materials. In addition, photomicrographs obtained using SEM (at 200x magnification) are shown in Figure 3. Based on the photomicrographs, it can be observed that the use of chitosan in B1 provided an enlargement in the porosity and pore sizes, as well as exhibited a morphology more regular than in B2 which is in good agreement with literature (Croisier & Jerome, 2013).

In vitro cytotoxicity tests

Using the agar diffusion method, the plates were macroscopically examined for the presence of a halo and were examined microscopically to determine the cellular integrity around the sample. Toxicity is confirmed by the presence of a clear halo around the material being tested. This halo is observed when cell death occurs, releasing neutral red dye into the cells and resulting in a clear area. The toxicity was evaluated by measuring the diameter of the formed inhibition halo. None of the biomaterials analyzed using the agar diffusion method exhibited toxicity; that is, no toxicity halo was observed around or under the samples, and the cells appeared unchanged, without any morphological alteration, and presenting identical behavior to the negative control. Analysis of the positive control showed a halo 13 mm in diameter around the latex sample, confirming the inherent toxicity of this material as observed by the cell lysis. In this regard, a cell vitality control was performed: In the absence of biomaterials, the effects of the diffusion components originating from the materials were evaluated by placing these components in indirect contact with the cells. In this test, a small layer of agar separated the cells from the materials, alleviating the cytotoxic effect of the materials on the sol-gel and consequently creating an additional diffusion barrier. This test mimics the effects of the cell response close but not directly adjacent to the materials (Nablo & Schoenfisch, 2005). Therefore, cells that were very close to the sample appeared unaltered and remained alive, indicating the non–toxic nature of the evaluated biomaterials.

Using the method of diffusing an extract in solution, the cytotoxicity tests were carried out using biomaterial extracts (see Figure 4). The results of this test were similar to those found using the agar diffusion method. The three evaluated biomaterials and the negative control showed no cell toxicity, regardless of the concentration used. Only the positive control showed a toxic effect on the evaluated cell lines, especially at higher concentrations. Notably, calcium phosphate cements are non–toxic (Carey, Xu, Simon Jr., Takagia, & Chow, 2005), and many of these composites have shown to promote cell adhesion and proliferation (Yuasa et al., 2004). The non–toxic nature of these biomaterials is due mainly to the similarity between the inorganic and bone constituents (Sun, Zhou, & Lee, 2011).

In vivo biocompatibility tests

For biomaterial B1, we observed (within three days) the presence of an acute inflammatory infiltrate containing a large number of lymphocytes and inflammatory cells. Examining the fibrous capsule, we observed conjunctive tissue with the moderate presence of fibroblasts and few blood vessels (see Figure 5, and Table 2). At seven days, in group B1, a lymphocyte–rich inflammatory infiltrate was still detected and also a greater number of fibroblasts and few blood vessels. At 28 days, there was a significant decrease in the number of lymphocytes, followed by an increase in the number of fibroblasts inside the biomaterial and in the presence of blood vessels, and the fibrous capsule appeared slightly denser.

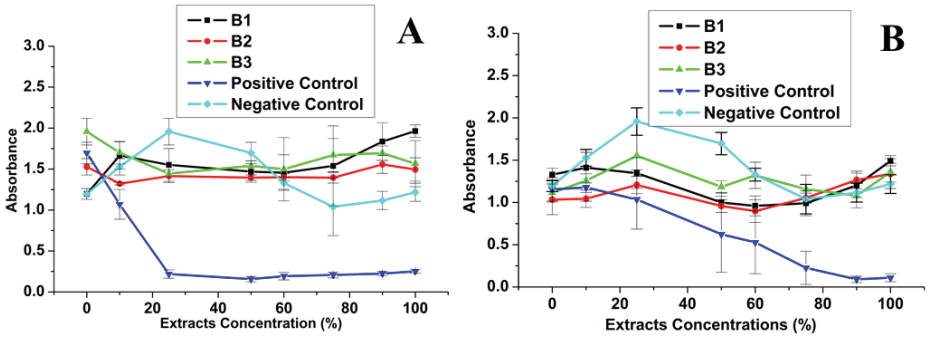

Figure 4. In vitro cytotoxicity test using the HEP (A) and VERO (B) cell lines.

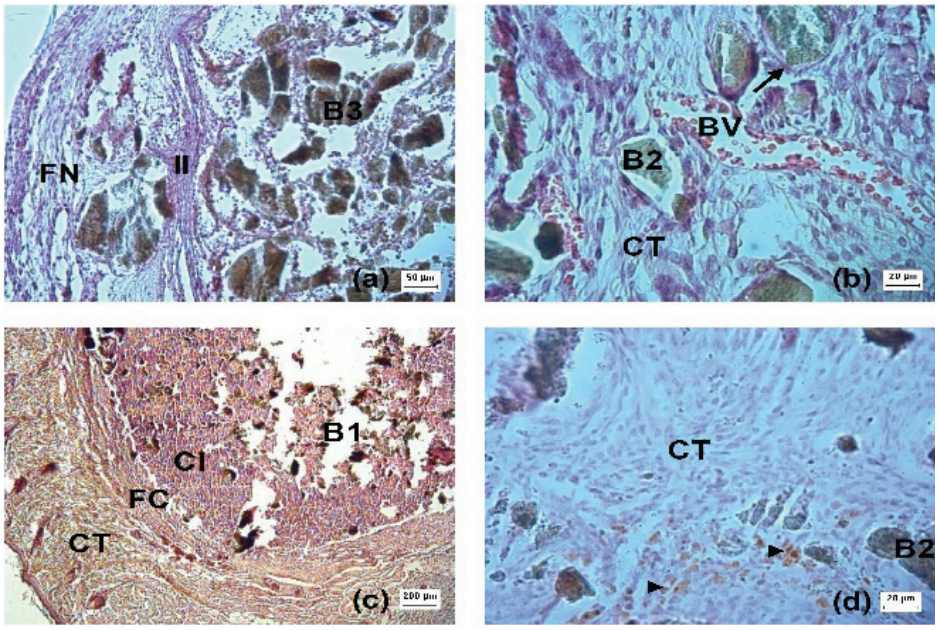

Figure 5. Representative photomicrographs of the subcutaneous tissue surrounding the implants for illustration of the hystomorphometric findings. (a) On day 3 a fibrin network (FN) has been formed around biomaterial 3 (B3) within an inflammatory infiltration (II) of polymorphnuclear cells, lymphocytes and macrophages (magnification: 200x). (b) On day 7 biomaterial 2 (B2) has been surrounded by a connective tissue (CT) with fibroblasts (arrow) integrated on implants. Blood vessels (BV) were numerously present close to the biomaterial. (magnification: 500x). (c) On day 28 a thin fibrous capsule (FC) surrounded the biomaterial 1 (B1) was found. An important cellular ingrowth (CI) regenerating the connective tissue (CT) (magnification: 50x). (d) On day 28 a regenerated connective tissue (CT) shows few macrophages (arrow heads) surrounding the biomaterial 2 (B2). (magnification: 500x).

Table 2. The evaluation of the tissue response to the implants during the histological analyses for B1, B2 and B3 biomaterials*.

Tissue reaction to the implants	Biomaterials		
Inflammatory infiltrate	B1	B2	B3
3 days	(++++)	(+++)	(++)
7 days	(+++)	(++)	(+)
28 days	(+)	(+)	(+)
Fibrin network around the implant	B1	B2	B3
3 days	(+++)	(+++)	(+++)
7 days	(+++)	(++)	(++)
28 days	(++)	(+)	(-)
Neovascularization	B1	B2	B3
3 days	(-)	(-)	(-)
7 days	(-)	(-)	(+)
28 days	(+)	(++)	(+++)
Quality of the fibrous capsule	B1	B2	B3
3 days	(-)	(-)	(-)
7 days	(-)	(-)	(-)
28 days	(++)	(++)	(+)
Internal cell growth	B1	B2	B3
3 days	(-)	(-)	(-)
7 days	(-)	(+)	(++)
28 days	(+)	(++)	(+++)
Macrophages	B1	B2	B3
3 days	(-)	(-)	(-)
7 days	(-)	(-)	(-)
28 days	(++)	(++)	(+)

Biomaterial B2 showed inflammatory infiltrate at three days, with a moderate presence of lymphocytes and inflammatory cells. In initial days, the absence of a fibrous capsule and fibroblasts of the adjacent conjunctive tissue was also observed, leading to very close contact with the biomaterial. In contrast, at seven days, there was a significant decrease in the number of inflammatory cells, and at 28 days, few lymphocytes or macrophages were observed; in addition, many blood vessels were detected, and the biomaterial was integrated with the tissue. On the other hand, B3 presented little inflammatory infiltrate at three days and, at seven days, few lymphocytes were found, and blood vessels were adjacent to the biomaterial. At 28 days, the biomaterial B3 was in very close contact with the adjacent tissue, and many blood vessels were observed. In addition, an analysis of fibrin network also provided interesting results among these biomaterials. Among the three composites, the fibrin networks were high in the initial days, but it was detected an absence of fibrin at 28 days in B3, followed a moderate formation in B1 and a minor one in B2 at this stage. In this point, it is noteworthy to comment that fibroblast and vascular endothelial growth factors are the main aspects that influences the growth of new capillaries into the fibrin network, expressing macrophages and endothelial cells as a response to the composite interface, which consequently provides nutrients and oxygen to the new formed tissue (Schliephake, 2002).

Another important aspect of all biomaterials used in this study is that during the three-day period, an acute inflammatory reaction was observed in all the observed sections, and neutrophils and lymphocytes were abundant. This effect was more intense in group B1 than in the other groups. The acute inflammatory reaction was still presented at seven days, although, importantly, the reactions for all three materials were well within normal ranges, validating their applicability as biomaterials. In addition, after the 28–day period, lymphocytes and macrophages were found and exhibited greater numbers in group B1. This difference for group B1 is due to the acetyl groups of the remaining chitosan (both at 7 and 28 days).

Neovascularization and internal tissue growth were most prevalent in group B3, followed by groups B2 and B1, in that order. This vascularization was more noticeable in group B3, most likely due to the smaller size of the hydroxyapatite particles (Fischer, Layrolle, van Blitterswijk, & Bruijn, 2004; Tayton et al., 2014), which may lead into a more efficient release of calcium from small size particles (due to increased surface/volume ratio) that would result in stimulation of angiogenesis via calcium sensor (Castano et al., 2014). An important aspect of these findings is their relevance to the applicability of the biomaterials as scaffolds for tissue growth; this characteristic is attributed to the abundance of blood vessels observed around and inside the biomaterials.

Marked fragmentation of the implanted material was observed in all sections. At 28 days, it was possible to notice an apparent absorption of part of the material. This fragmentation is very important for new tissue formation. Fragmentation of the biomaterial is greatly stimulated by the collagen and/or chitosan polymer matrix, which is absorbed more rapidly than the mineral compound. The presence of few lymphocytes and the absence of granulomas at 28 days reflect low antigenicity, showing that no antigen or organic remnants remained inside of the material. The mild presence of a polymorphonuclear infiltrate at 28 days indicates the lack of persistent inflammatory stimuli; that is, most of the initial inflammation is due to the surgery itself.

Another aspect worth considering is the presence of newly-formed blood vessels. The presence of many newly-formed blood vessels intercalated with the compounds indicates an important vasculogenic stimulus by the biomaterials. Such stimuli are likely due to the bovine hydroxyapatite, which together with the collagen (or the chitosan) has characteristics that benefit tissue growth and osteoconduction (Ben-Nissan, 2003). A small number of macrophages and the absence of granulomas were observed, indicating that the compounds do not stimulate chronic inflammation, representing a good indication of biocompatibility. This result also shows that absorption of the compounds is facilitated by the organic matrix and by the small hydroxyapatite particles. Moreover, the small number of fibroblasts observed indicates that the compounds tend to be well absorbed (without the formation of fibrosis) and that the adjacent tissue suffers little alteration.

Conclusion

We conclude that the biomaterials evaluated in this study did not show *in vitro* cell toxicity. This lack of toxicity was established using both the agar diffusion method and the method of diffusing an extract in solution in both tested cell lines. While evaluating the response of subcutaneous tissue to the biomaterials, very mild inflammatory responses were observed enabling good internal tissue growth (which would be detrimental to their clinical applicability as tissue substitutes). The tissue response was most favorable for sample B3, followed by B2 and B1, in that order. Thus, the results obtained here indicate that the small hydroxyapatite particles are a key parameter and chitosan does not provide any advantage to the composite materials.

Acknowledgements

The authors thank the following funding agencies for their financial support: CNPq (*Conselho Nacional de Desenvolvimento Científico e Tecnológico*), Fapesp (*Fundação de Amparo à Pesquisa do Estado de São Paulo*) and Capes (*Coordenação de Aperfeiçoamento de Pessoal de Nível Superior*). We would also like to thank prof. Dr. Sérgio B. Garcia (USP, Ribeirão Preto, State São Paulo), Dr. Virgínia C. A. Martins (USP, São Carlos, State São Paulo), the Laboratory of Biochemistry and Biomaterials of the São Carlos Institute of Chemistry (IQSC-USP), the bioengineering laboratory of the São Carlos School of Engineering (USP), the biochemistry and cell culture laboratories of IQSC-USP and the cancer pathology laboratory of the School of Medicine of Ribeirão Preto (FMRP-USP).

References

Attaf, B. (2011). *Advances in composite materials for medicine and nanotechnology*. Shanghai, CN: InTech China.

Begam, H., Nandi, S. K., Chanda, A., & Kundu, B. (2017). Effect of bone morphogenetic protein on Zn-HAp and Zn-HAp/collagen composite: A systematic in vivo study. *Research in Veterinary Science, 115*, 1-9. doi: 10.1016/j.rvsc.2017.01.012

Ben-Nissan, B. (2003). Natural bioceramics: from coral to bone and beyond. *Current Opinion in Solid State and Materials Science, 7*(4-5), 283-288. doi: 10.1016/j.cossms.2003.10.001

Bongio, M., van den Beucken, J. J. J. P., Leeuwenburgh, S. C. G., & Jansen, J. A. (2015). Preclinical evaluation of injectable bone substitute materials. *Journal of Tissue Engineering and Regenerative Medicine, 9*(3), 191-209. doi: 10.1002/term.1637

Calabrese, G., Giuffrida, R., Forte, S., Fabbi, C., Figallo, E., Salvatorelli, L., ... Gulino, R. (2017). Human adipose-derived mesenchymal stem cells seeded into a collagen-hydroxyapatite scaffold promote bone

augmentation after implantation in the mouse. *Scientific Reports, 7*(1), 7110. doi: 10.1038/s41598-017-07672-0

Carey, L. E., Xu, H. H. K., Simon Jr., C. G., Takagia, S., & Chow, L. C. (2005). Premixed rapid-setting calcium phosphate composites for bone repair. *Biomaterials, 26*(24), 5002-5014. doi: 10.1016/j.biomaterials.2005.01.015

Castano, O., Sachot, N., Xuriguera, E., Engel, E., Planell, J. A., Park, J. H., ... Kim, H. W. (2014). Angiogenesis in bone regeneration: tailored calcium release in hybrid fibrous scaffolds. *ACS Aplied Materials and Interfaces, 6*(10), 7512-7522. doi: 10.1021/am500885v

Chen, Y., Songjian, L., Xiaoming, L., Zhang, Y., Huang, Z., Feng, Q., ... Yu, B. (2012). Noninvasive evaluation of injectable chitosan/nano-hydroxyapatite/collagen scaffold via ultrasound. *Journal of Nanomaterials, 2012*, 939821. doi: 10.1155/2012/939821

Choi, J.-W., Kim, J.-W., Jo, I.-H., Koh, Y.-H., & Kim, H.-E. (2017). Novel self-assembly-induced gelation for nanofibrous collagen/hydroxyapatite composite microspheres. *Materials, 10*(10), 1110. doi: 10.3390/ma10101110

Croisier, F., & Jerome, C. (2013). Chitosan-based biomaterials for tissue engineering. *European Polymer Journal, 49*(4), 780-792. doi: 10.1016/j.eurpolymj.2012.12.009

Fischer, E. M., Layrolle, P., van Blitterswijk, C. A., & Bruijn, J. D. (2004). Bone formation by mesenchymal progenitor cells cultured on dense and microporous hydroxyapatite particles. *Tissue Engineering, 9*(6), 1179-1188. doi: 10.1089/10763270360728080

Goissis, G., Piccirilli, L., Plepis, A. M. G., & Das-Gupta, D. K. (1999). Preparation and characterization of anionic collagen: P(VDF/TrFE) composites. *Polymer Engineering & Science, 39*(3), 474-482. doi: 10.1002/pen.11437

Horn, M. M., Martins, V. C. A., & Plepis, A. M. G. (2009). Interaction of anionic collagen with chitosan: Effect on thermal and morphological characteristics. *Carbohydrate Polymers, 77*(2), 239-243. doi: 10.1016/j.carbpol.2008.12.039

Horn, M. M., Martins, V. C. A., & Plepis, A. M. G. (2010). Determination of activation energy in polymeric hydrogels using thermogravimetric analysis. *Polimeros, 20*(3), 201-204. doi: 10.1590/S0104-14282010005000025

Huang, Z., Chen, Y., Feng, Q. L., Zhao, W., Yu, B., Tian, J., ... Lin, B.-M. (2011a). *In vivo* bone regeneration with injectable chitosan/hydroxyapatite/collagen composites and mesenchymal stem cells. *Frontiers of Materials Science, 5*(3), 301-310. doi: 10.1007/s11706-011-0142-4

Huang, Z., Feng, Q., Yu, B., & Li, S. (2011b). Biomimetic properties of an injectable chitosan/nano-hydroxyapatite/ collagen composite. *Materials Science and Engineering C, 31*(3), 683-687. doi: 10.1016/j.msec.2010.12.014

Huang, Z., Yu, B., Feng, Q., Li, S., Chen, Y., & Luo, L. (2011c). In situ-forming chitosan/nano-hydroxyapatite/collagen gel for the delivery of bone marrow mesenchymal stem cells. *Carbohydrate Polymers, 85*(1), 261-267. doi: 10.1016/j.carbpol.2011.02.029

Huang, Z., Tian, J., Yu, B., Xu, Y., & Feng, Q. (2009). A bone-like nano-hydroxyapatite/ collagen loaded injectable scaffold. *Biomedical Materials, 4*(5), 055005. doi: 10.1088/1748-6041/4/5/055005

Jing, Z., Wu, Y., Su, W., Tian, M., Jiang, W., Cao, L., ... Zhao, Z. (2017). Carbon nanotube reinforced collagen/hydroxyapatite scaffolds improve bone tissue formation *in vitro* and *in vivo*. *Annals of Biomedical Engineering, 45*(9), 2075-2087. doi: 10.1007/s10439-017-1866-9

Kaczmarek, B., Sionkowsk, A., & Osyczka, A. M. (2017). The comparison of physic-chemical properties of chitosan/collagen/hyaluronic acid composites with nano-hydroxyapatite cross-linked by dialdehyde starch and tannic acid. *Polymer Testing, 62*, 171-176. doi: 10.1016/j.polymertesting.2017.06.027

Keranen, P., Moritz, N., Alm, J. J., Ylänen, H., Kommonen, B., & Aro, H. T. (2011). Bioactive glass microspheres as osteopromotive inlays in macrotextured surfaces of Ti and CoCr alloy bone implants: Trapezoidal surface grooves without inlay most efficient in resisting torsional forces. *Journal of the Mechanical Behavior of Biomedical Materials, 4*(7), 1483-1491. doi: 10.1016/j.jmbbm.2011.05.018

Kozlowska, J., Sionkowska, A., Osyczka, A. M., & Dubiel, M. (2017). Stabilizing effect of carbodiimide and dehydrothermal treatment crosslinking on the properties of collagen/hydroxyapatite scaffolds. *Polymer International, 66*(8), 1164-1172. doi: 10.1002/pi.5371

Li, R. W., Chow, T. W., & Matinlinna, J. P. (2014). Ceramic dental biomaterials and CAD/CAM technology: state of the art. *Journal of Prosthodontic Research, 58*(4), 208-216. doi: 10.1016/j.jpor.2014.07.003

Nablo, B. J., & Schoenfisch, M. K. (2005). *In vitro* cytotoxicity of nitic oxide-releasing sol-gel derived materials. *Biomaterials, 26*(21), 4405-4415. doi: 10.1016/j.biomaterials.2004.11.015

Ong, K., Yun, M., & White, J. (2015). New biomaterials for orthopedic implants. *Orthopedic Research and Reviews, 2015*(7), 107-130. doi: 10.2147/ORR.S63437

Quinlan, E., Lopez-Noriega, A., Thompson, E., Kelly, H. M., Cryan, S. A., & O´Brien, F. J. (2015). Development of collagen–hydroxyapatite scaffolds incorporating PLGA and alginate microparticles for the controlled delivery of rhBMP-2 for bone tissue engineering. *Journal of Controlled Release, 198*, 71-79. doi: 10.1016/j.jconrel.2014.11.021

Rogero, S. O., Lugao, A. B., Ikeda, T. I., & Cruz, A. S. (2003). Teste *in vitro* de citotoxicidade: estudo comparativo entre duas metodologias. *Material Research, 6*(3), 317-320. doi: 10.1590/S1516-14392003000300003]

Rogero, S. O., Higa, O. Z., Saiki, M., Correa, O. V., & Costa, I. (2000). Cytotoxicity due to corrosion of ear piercing studs. *Toxicology in Vitro, 14*(6), 497-504. doi: 10.1016/S0887-2333(00)00047-3

Sadat-Shojai, M., Khorasani, M.-T., Dinpanah-Khoshdargi, E., & Jamshidi, A. (2013). Synthesis methods for nanosized hydroxyapatite with diverse structures. *Acta Biomaterialia, 9*(8), 7591-7621. doi: 10.1016/j.actbio.2013.04.012

Sari, N. K., Indrani, D. J., Johan, C., & Corputty, J. E. M. (2017). Evaluation of chitosan-hydroxyapatite-collagen composite strength as scaffold material by immersion in simulated body fluid. *Journal of Physics: Conferences Series, 884*(1), 012116. doi: 10.1088/1742-6596/884/1/012116

Sato, T., Kikuchi, M., & Aizawa, M. (2017). Preparation of hydroxyapatite/collagen injectable bone paste with an anti-washout property utilizing sodium alginate. Part 1: influences of excess supplementation of calcium compounds. *Journal of Materials Science: Materials in Medicine, 28*(3), 49. doi: 10.1007/s10856-017-5853-3

Schliephake, H. (2002). Bone growth factors in maxillofacial skeletal reconstruction. *International Journal of Oral and Maxillofacial Surgery, 31*(5), 469-484. doi: 10.1054/ijom.2002.0244

Shin, H. (2007). Fabrication methods of an engineered microenvironment for analysis of cell–biomaterial interactions. *Biomaterials, 28*(2), 126-133. doi: 10.1016/j.biomaterials.2006.08.007

Sionkowsk, A., & Kaczmarek, B. (2017). Preparation and characterization of composites based on the blends of collagen, chitosan and hyaluronic acid with nano-hydroxyapatite. *International Journal of Biological Macromolecules, 102*, 658-666. doi: 10.1016/j.ijbiomac.2017.03.196

Sun, F., Zhou, H., & Lee, J. (2011). Various preparation methods of highly porous hydroxyapatite/polymer nanoscale biocomposites for bone regeneration. *Acta Biomaterialia, 7*(11), 3813-3828. doi: 10.1016/j.actbio.2011.07.002

Taylor, J. C., Cuff, S. E., Leger, J. P., Morra, A., & Anderson, G. I. (2002). *In vitro* osteoclast resorption of bone substitute biomaterials used for implant site augmentation: a pilot study. *International Journal of Oral and Maxillofacial Surgery, 17*(3), 321-330.

Taylor, L. R., Papp, R. B., & Pollard, B. D. (1994). *Instrumental methods for determining elements*. New York, NY: VCH Published.

Tayton, E., Purcell, M., Aarvold, A., Smith, J. O., Briscoe, A., Kanczler, J. M., & Oreffo, R. O. (2014). A comparison of polymer and polymer–hydroxyapatite composite tissue engineered scaffolds for use in bone regeneration. an in vitro and in vivo study. *Journal of Biomedical Materials Research Part A, 102*(8), 2613-2624. doi: 10.1002/jbm.a.34926

Teng, S. H., Liang, M. H., Wang, P., & Luo, Y. (2016). Biomimetic composite microspheres of collagen/chitosan/nano-hydroxyapatite: In-situ synthesis and characterization. *Materials Science and Engineering: C, 58*(1), 610-613. doi: 10.1016/j.msec.2015.09.021

Verisqa, F., Triaminingsih, S., & Corputty, J. E. M. (2017). Composition of chitosan-hydroxyapatite-collagen composite scaffold evaluation after simulated body fluid immersion as reconstruction materia. *Journal of Physics: Conf. Series, 884*(1), 012035. doi: 10.1088/1742-6596/884/1/012035

Wang, J., Zhang, Z., Su, G., Xiaomin, S., Yingying, W., Zhexiang, F., & Qiqing, Z. (2017). Graphene oxide incorporated collagen/nano-hydroxyapatite composites with improved mechanical properties for bone

repair materials. *Journal of Biomaterials and Tissue Engineering, 7*(10), 1000-1007. doi: 10.1166/jbt.2017.1657

Yuasa, T., Miyamoto, Y., Ishikawa, K., Takechi, M., Momota, Y., Tatehara, S., & Nagayama, M. (2004). Effects of apatite cements on proliferation and differentiation of human osteoblasts *in vitro*. *Biomaterials, 25*(7-8), 1159-1166. doi: 10.1016/j.biomaterials.2003.08.003

Zhao, X., Li, H., Xu, Z., Li, K., Cao, S., & Jiang, G. (2017). Selective preparation and characterization of nano-hydroxyapatite/collagen coatings with three-dimensional network structure. *Surface and Coatings Technology, 332*, 227-237. doi: 10.1016/j.surfcoat.2017.05.042

Zhou, H., & Lee, J. (2011). Nanoscale hydroxyapatite particles for bone tissue engineering. Acta Biomaterialia, 7(n. 7), 2769-2781. doi: 10.1016/j.actbio.2011.03.019